Rajshahi University journal of science and engineering **ISSN 2309-0952 (Print)**
Vol. 46-53 (2018-2025), pp 51- 67 **ISSN 2408-8803 (Online)**
DOI: https://doi.org/10.64102/rujse.0765

Analyzing the Co-Dynamics of COVID-19 Strains with Early Detection Through the Fractional Laplace Adomian Decomposition Method

Sharmin Sultana Shanta[1*], Md. Abul Kalam Azad[2]

Abstract

The emergence of multiple COVID-19 strains has been the greatest challenge since the initial outbreak. A fractional-order mathematical model is formulated to investigate the co-dynamics of multiple COVID-19 strains with memory effects through the Caputo fractional derivative. The model is based on an extended SEIR framework including two exposed parameters named as early detection to quarantine compartments to reflect realistic intervention strategies. Fractional Laplace Adomian Decomposition Method (FLADM) has been used to solve the resulting system and analyzed the behavior for various values of the fractional order α. The results show strong agreement between LADM and the fractional Runge-Kutta fourth-order method at $\alpha = 0.7$ which is indicating the accuracy and efficiency of our approach. This model provides a refined perspective on short-term epidemic scenarios by capturing the memory-dependent nature of disease transmission and intervention by offering valuable insights for public health planning and control strategies.

Keywords: Fractional Laplace Adomian decomposition method (LADM); Runge-Kutta fourth-order method (RK4); numerical solution; Covid-19 strains;

1 Introduction

The Coronavirus Disease 2019 (COVID-19) was caused by the novel severe acute respiratory syndrome coronavirus 2 (SARS-CoV-2), which emerged in late 2019 and rapidly caused consternation among the people and became a global pandemic (World Health Organization [WHO], n.d.). COVID-19, identified as high transmissible, diverse clinical outcomes, and assorted incubation periods, has exhausted healthcare systems (Centers for Disease Control and Prevention [CDC], 2023). Over time, multiple variants of COVID-19 have emerged that pose a threat to the health system (Chang et al., 2021) and the human immune system (Chowdhury et al., 2020). The strains of those variants have made adjustment efforts more challenging (Jacobs et al., 2023). To forecast disease dynamics and assess the effectiveness of control strategies, adaptive and accurate modeling tools are necessary (Thompson, 2020). The pioneer of Mathematical modeling of infectious diseases was Kermack and McKendrick, who introduced the classical SIR model. This model is divided into three classes-susceptible (S), infected (I), and recovered (R), and is described in a system of ordinary differential equations to analyze the transmission dynamics of a disease. Their work is identified as the first mathematical framework to understand the flow of epidemics and remains a cornerstone of theoretical epidemiology (Kermack &

[1] M.Phil Researcher, Department of Applied Mathematics, University of Rajshahi, Rajshahi 6205, Bangladesh; Assistant Professor, Mathmatics Descipline, Khulna University, Khulna 9208, Bangladesh; E-mail: shanta@math.ku.ac.bd * Corresponding Author

[2] Professor, Department of Applied Mathematics, University of Rajshahi, Rajshahi 6205, Bangladesh; E-mail: azad267@gmail.com

McKendrick, 1927). Later on time, many researchers identify the latent period which was added in the classical SIR model and it was extended into the SEIR model, which includes an exposed compartment to represent individuals who are infected but not symptomatic. The primal SEIR model was studied about the measles outbreaks in 1984 (Aron & Schwartz, 1984). Since then, the SEIR structure has achieved a standard framework for modeling diseases like monkey pox (Bentaleb et al., 2024), dengue (Bhuju et al., 2022), ebola (Islam et al., 2024), influenza (Ali et al., 2024), and many other diseases where individuals experience an incubation period before becoming infectious. Since its initial development, the SEIR model has multiple modifications and expansions to reflect the complexities of real-world disease dynamics. These extensions include with additional compartments - such as asymptomatic (Huo et al., 2021), hospitalized (Heim et al., 2019), quarantined (Safi & Gumel, 2011), or vaccinated (White et al., 2015) individuals as well as time delays (Prakash Raj et al., 2025), stochastic effects (Upadhyay et al., 2025), spatial heterogeneity (Zhang et al., 2025), and fractional-order derivatives (Minhós et al., 2025). Such assimilation allows the model to capture the transmission patterns, intervention strategies, and biological characteristics of various infectious diseases more accurately. Since the beginning of the COVID-19 pandemic, many mathematical models have been proposed to identify the transmission dynamics and support policy decisions. The earliest SEIR-based model was formulated in 2020 to forecast the initial outbreak of COVID-19 in Wuhan, and estimates of the basic reproduction number (Wu et al., 2020). Another model was constructed with an extended SEIR model for undetected infections that focused on the importance of asymptomatic and undocumented cases (Ivorra et al., 2020). Multiple models have been developed to visualize the 2 prospect of minimizing the spread of disease by employing lockdown (Ghosh et al., 2022), sufficient hospital resource management (Redondo et al., 2023), and extensive public health interventions (Mondal & Khajanchi, 2022). A non-autonomous system has been developed to identify the impact of temperature on disease transmission, simulations manifest that the epidemic can be controlled with a vaccination rate of 70%. However, safety measures and sensitizing populations to hygiene rules become vital when vaccination coverage is below 70% (Abraham et al., 2025). The emergence of new SARS-CoV-2 variants has complicated the trajectory of the pandemic era. Every variant has unique challenges with increasing transmissibility, immune evasion, and impacts on vaccine efficacy. For instance, the Delta variant was found to be 65−90% more transmissible than the Alpha variant, leading to substantial surges in cases and hospitalizations (Panovska-Griffiths et al., 2022). A compartmental model has been formulated to analyze the transmission dynamics of COVID-19 and focused on the Delta and Omicron variants in India with model the key factors such as vaccination, time-dependent transmission, economic burden, loss of immunity, and asymptomatic recovery to established epidemiological insights (Negi et al., 2024). A two-strain mathematical framework for the B.1.1.7 variant infections has been formulated to estimate a mutant strain. The Model was fitted with data of Ontario glorify variant dominance and highlight that interventions alongside vaccination can prevent the resurgence (Betti et al., 2021). The emergence of COVID-19 variants like Alpha, Beta, Gamma, and Delta presents serious global health challenges. A precise model has been glorified with time-dependent vaccination rates that applied for India’s multi-variant

scenario to confirm the combined strategy act as most effective also offering cost-efficient, with data-driven guidance for pandemic response (Ambalarajan et al., 2025). Traditional integer-order epidemiological models often assume the future state of an epidemic depends its current conditions and neglect the influence of past events but real-world disease dynamics frequently exhibit memory effects, where previous exposures, recoveries, and interventions impact current transmission rates (Agarwal et al., 2024, Barros et al., 2021). COVID-19 mainly caused by a mutagenic RNA virus, has seen the emergence of transmissible variants since late 2020. This study offering a two strain computational model for South Africa and Caputo fractional derivatives and non-standard finite difference schemes has been applied for simulation. Outcomes analyzed the WHO-recommended SOPs influences that reduce the infection across different strain scenarios (Riaz et al., 2025). A fractional-order model has been constructed to simulate the dynamics of a three-strain influenza outbreak with treatment strategies which can magnificently reduce infection levels (Yaagoub et al., 2025). A fractional-order 3 SIRS model for Delta and Omicron has explored to describe COVID-19 dynamics with horizontal transmission and immunity loss to estimate the epidemic peak for Delta which was demonstrating the utility of fractional calculus in epidemic modeling (Bouissa et al., 2025). There have several well-established analytical and semi-analytical methods for solving fractional differential equations (FDEs) such as the Homotopy Perturbation Method (HPM) (Islam & Akbar, 2024), Variational Iteration Method (VIM) (Abdulrhman, 2025), Differential Transform Method (DTM) (Chu et al., 2024), Laplace Adomian Decomposition Method (LADM) (Saber et al., 2025) and many others. Here, we have adopted the Laplace Adomian Decomposition Method (LADM) combined by the Laplace transformation to handle the initial conditions and simplify fractional derivatives with the Adomian Decomposition Method, which systematically handles nonlinearities. A fractional-order model of smoking cessation dynamics has been formulated and analyzed by LADM to find graphical results. The solution technique has been compared with the RK4 method to demonstrate its accuracy (Haq et al., 2018). LADM has been used in a Caputo fractional-order HIV and COVID-19 co-dynamics model and investigate on treatment policies, immune response and disease transmission rate (Baba et al., 2024). Caputo derivative based fractional-order SEIR framework of measles transmission has formulated and LADM applied to trace the solutions at various fractional orders (Farman et al., 2018). Though several studies have investigated the transmission dynamics of COVID 19 using classical and fractional-order models, many have either neglected the presence of multiple strains or overlooked critical intervention compartments such as early detection or self-quarantine. On the other hand, a few studies have compared analytical methods like the LADM with numerical schemes such as the fractional RK4 technique to validate solution accuracy. Motivated by these gaps, this study develops a fractional-order co-dynamics model for multiple COVID-19 strains by extending an existing SEIR framework with two new parameters that flow from exposed individuals to quarantine to reflect the real-world intervention measures. We will use LADM and compare them with numerical results to demonstrate the method's effectiveness. This work aims to enhance the realism and analytical tractability of COVID-19 modeling, particularly for short-term outbreak scenarios where memory effects are significant.

2 Model Description

We have taken the model of Kim et al. (2024), which was formulated to observe the dynamics of COVID-19 strains within a population using an integer compartmental framework. This model divides the population into seven epidemiological classes, including susceptible individuals, exposed individuals for strains 1 and 2, infectious individuals for strains 1 and 2, quarantined individuals, and recovered individuals. All the compartments are denoted as $S(\mathrm{t}), \mathrm{E}_1(\mathrm{t}), \mathrm{E}_2(\mathrm{t}), \mathrm{I}_1(\mathrm{t}), \mathrm{I}_2(\mathrm{t}), Q(\mathrm{t})$, and $R(t)$ respectively where two parameters β_1 and β_2 illustrate transmission rates from S to E_1 and E_2, interact with I_1 and I_2. The movement of E_1 to I_1 is σ_1, whereas the movement of E_2 to I_2 is σ_2. Both these motions show the expansion of infections. Infected individuals $(\mathrm{I}_1, \mathrm{I}_2)$ move to the quarantine Q at rates τ_1 and τ_2. Quarantined individuals Q gets recovery with a rate θ and stays in R class. However, undetected individuals get their natural recovery with two rates γ_1 and γ_2, and leave I_1 and I_2 and move to R. This R class can collapse their immunity and eventually move back to S with ν rate.

This study focuses a short-term scenario to analyze the co-dynamics of multiple COVID-19 strains. To better capture the real-world dynamics of COVID-19 control measures, we have extended the original model by introducing two additional parameters that control the movement of individuals from the exposed $E_1(t)$ and $E_2(t)$ compartments to the quarantine $Q(t)$ compartment. The modifications of this model aimed to emphasize the impact of early detection of exposed (but not yet infectious) individuals.

The newly introduced parameters are defined as follows:

ϕ_1 : The rate of individuals who are exposed for strain 1 and transferred to quarantine.

ϕ_2 : The rate of individuals who are exposed for strain 2 and transferred to quarantine.

These additional parameters help the model reflect public health interventions such as early detection to avoid high-risk contacts. Combining the parameters and their assumptions in the model of Kim et al. (2024), we get the following system:

$$\begin{aligned}
S'(t) &= -\beta_1 S(t) I_1(t) - \beta_2 S(t) I_2(t) + \nu R(t),\\
E_1'(t) &= \beta_1 S(t) I_1(t) - (\phi_1 + \sigma_1) E_1(t),\\
E_2'(t) &= \beta_2 S(t) I_2(t) - (\phi_2 + \sigma_2) E_2(t),\\
I_1'(t) &= \sigma_1 E_1(t) - (\delta + \tau_1 + \gamma_1) I_1(t),\\
I_2'(t) &= \sigma_2 E_2(t) - (\delta + \tau_2 + \gamma_2) I_2(t),\\
Q'(t) &= \tau_1 I_1(t) + \phi_1 E_1(t) + \tau_2 I_2(t) + \phi_2 E_2(t) - \theta Q(t),\\
R'(t) &= \theta Q(t) + \gamma_1 I_1(t) + \gamma_2 I_2(t) - \nu R(t).
\end{aligned} \tag{2.1}$$

With initial conditions:

$$\begin{aligned}
&S(0) = S_0 \geq 0, && E_2(0) = E_{20} \geq 0, && I_2(0) = I_{20} \geq 0,\\
&E_1(0) = E_{10} \geq 0, && I_1(0) = I_{10} \geq 0, && Q(0) = Q_0 \geq 0,\\
& && && R(0) = R_0 \geq 0.
\end{aligned} \tag{2.2}$$

And total population,

$$N(t) = S(t) + E_1(t) + E_2(t) + I_1(t) + I_2(t) + Q(t) + R(t).$$

To analyze the memory and hereditary properties for real-world disease transmission, we have extended the classical integer-order model (2.1) using Caputo fractional derivatives. The transmission way of COVID-19 is vastly relevant with the latency periods, long-term immunity effects, and delays in symptom. By using the Caputo derivative of order $\alpha \in (0,1]$, we are introducing a non-local temporal operator that reflects these real-world effects. Additionally, this fractional-order approach provides a flexible framework, where the model interpolates between classical dynamics $\alpha = 1$ and systems with strong memory effects for $\alpha < 1$. In this study, we examine the model under different values of α to explore the impact of memory on the co-dynamics of COVID-19 strains and demonstrate how the fractional model enhances both the realism and accuracy of the predictions. The modified model after using the Caputo fractional derivative is compactly as follows:

$$D_t^{\alpha_i}\mathbf{x}(t) = \mathbf{F}(t, \boldsymbol{\mu}, \mathbf{x}) \tag{2.3}$$

where

$\mathbf{x} \in \mathbb{R}^n$ represents the states of model (2.1), $\boldsymbol{\mu} \in \mathbb{R}^m$ denotes the set of the associated parameters, and $\mathbf{F}(t, \boldsymbol{\mu}, \mathbf{x})$ is the (flow) right-hand side of model (2.1). Moreover, α_i denotes α_1 to α_7.

The initial conditions for model (2.3) are given by:

$$\mathbf{x}(0) = p_i \geq 0, \text{ where } i = 1 \ldots 7 \tag{2.4}$$

3 Conceptual Evaluation

To solve the modified fractional-order co-dynamics model, we employed the LADM for its efficiency in handling nonlinear fractional differential equations. LADM merges the Laplace transform with Adomian decomposition to yield semi-analytical which can rapidly converging series solutions. This approach preserves the model's nonlinear and memory-dependent structure while remaining computationally efficient and easy to implement.

3.1 Numerical Approach via FLADM

$$L\{D_t^{\alpha_i}\mathbf{x}(t)\} = L\{\mathbf{F}(t, \boldsymbol{\mu}, \mathbf{x})\} \tag{3.1}$$

Applying Laplace transformation, (3.1) becomes

$$s^{\alpha_i} L\{\mathbf{x}(t)\} - s\,\mathbf{x}(0) = L\{\mathbf{F}(t, \boldsymbol{\mu}, \mathbf{x})\} \tag{3.2}$$

Applying the Laplace transformation with initial conditions (2.4) in Eq. (3.2) becomes

$$\begin{aligned}
&L\{S(t)\} = p_1 s^{-1} + s^{-\alpha_1}[L\{-\beta_1 S(t)I_1(t) - \beta_2 S(t)I_2(t) + \nu R(t)\}],\\
&L\{E_1(t)\} = p_2 s^{-1} + s^{-\alpha_2}[L\{\beta_1 S(t)I_1(t) - (\phi_1 + \sigma_1)E_1(t)\}],\\
&L\{E_2(t)\} = p_3 s^{-1} + s^{-\alpha_3}[L\{\beta_2 S(t)I_2(t) - (\phi_2 + \sigma_2)E_2(t)\}],\\
&L\{I_1(t)\} = p_4 s^{-1} + s^{-\alpha_4}[L\{\sigma_1 E_1(t) - (\delta + \tau_1 + \gamma_1)I_1(t)\}],\\
&L\{I_2(t)\} = p_5 s^{-1} + s^{-\alpha_5}[L\{\sigma_2 E_2(t) - (\delta + \tau_2 + \gamma_2)I_2(t)\}],\\
&L\{Q(t)\} = p_6 s^{-1} + s^{-\alpha_6}[L\{\tau_1 I_1(t) + \phi_1 E_1(t) + \tau_2 I_2(t) + \phi_2 E_2(t) - \theta Q(t)\}],\\
&L\{R(t)\} = p_7 s^{-1} + s^{-\alpha_7}[L\{\theta Q(t) + \gamma_1 I_1(t) + \gamma_2 I_2(t) - \nu R(t)\}].
\end{aligned} \tag{3.3}$$

Therefore, the solution can be presented by an infinite series as follows:

$$S(t)=\sum_{n=0}^{\infty}s_n,\quad E_2(t)=\sum_{n=0}^{\infty}e_{2n},\quad I_2(t)=\sum_{n=0}^{\infty}i_{2n},\quad R(t)=\sum_{n=0}^{\infty}r_n. \tag{3.4}$$
$$E_1(t)=\sum_{n=0}^{\infty}e_{1n},\quad I_1(t)=\sum_{n=0}^{\infty}i_{1n},\quad Q(t)=\sum_{n=0}^{\infty}q_n,$$

The infinite series of nonlinear terms $S_n(t)I_{1n}(t)$ and $S_n(t)I_{2n}(t)$ are:

$$S(t)I_1(t)=\sum_{n=0}^{\infty}M_n,\qquad S(t)I_2(t)=\sum_{n=0}^{\infty}N_n. \tag{3.5}$$

Thus the Adomian polynomials are:

$$M_n=\frac{1}{\Gamma(n+1)}\frac{d^n}{d\Phi^n}\left[\sum_{q=0}^{n}\Phi^q I_{1q}(t)\sum_{q=0}^{n}\Phi^q S_q(t)\right],$$
$$N_n=\frac{1}{\Gamma(n+1)}\frac{d^n}{d\Lambda^n}\left[\sum_{q=0}^{n}\Lambda^q I_{2q}(t)\sum_{q=0}^{n}\Lambda^q S_q(t)\right].$$

Now, substituting the series (3.4) and (3.5) in eq. (3.3), we get,

$$L\{\sum_{n=0}^{\infty}S_{n+1}(t)\}=p_1s^{-1}-s^{-\alpha_1}L\{-\beta_1\sum_{n=0}^{\infty}M_n-\beta_2\sum_{n=0}^{\infty}N_n+\nu R_n(t)\},$$
$$L\{\sum_{n=0}^{\infty}E_{1(n+1)}(t)\}=p_2s^{-1}+s^{-\alpha_2}L\{\beta_1\sum_{n=0}^{\infty}M_n-(\phi_1+\sigma_1)E_{1n}(t)\},$$
$$L\{\sum_{n=0}^{\infty}E_{2(n+1)}(t)\}=p_3s^{-1}+s^{-\alpha_3}L\{\beta_2\sum_{n=0}^{\infty}N_n-(\phi_2+\sigma_2)E_{2n}(t)\},$$
$$L\{\sum_{n=0}^{\infty}I_{1(n+1)}(t)\}=p_4s^{-1}+s^{-\alpha_4}L\{\sigma_1E_{1n}(t)-(\delta+\tau_1+\gamma_1)I_{1n}(t)\}, \tag{3.6}$$
$$L\{\sum_{n=0}^{\infty}I_{2(n+1)}(t)\}=p_5s^{-1}+s^{-\alpha_5}L\{\sigma_2E_{2n}(t)-(\delta+\tau_2+\gamma_2)I_{2n}(t)\},$$
$$L\{\sum_{n=0}^{\infty}Q_{n+1}(t)\}=p_6s^{-1}+s^{-\alpha_6}L\{\tau_1I_{1n}(t)+\phi_1E_{1n}(t)+\tau_2I_{2n}(t)+\phi_2E_{2n}(t)-\theta Q_n(t)\},$$
$$L\{\sum_{n=0}^{\infty}R_{n+1}(t)\}=p_7s^{-1}+s^{-\alpha_7}L\{\theta Q_n(t)+\gamma_1I_{1n}(t)+\gamma_2I_{2n}(t)-\nu R_n(t)\}.$$

Now, evaluating Eq. (3.2) along with the expressions (3.3) and (3.6) and enforce the inverse Laplace on two sides, we obtain

$$\sum_{n=0}^{\infty}S_{n+1}(t)=p_1-L^{-1}[s^{-\alpha_1}L\{-\beta_1\sum_{n=0}^{\infty}M_n-\beta_2\sum_{n=0}^{\infty}N_n+\nu R_n(t)\}],$$
$$\sum_{n=0}^{\infty}E_{1(n+1)}(t)=p_2+L^{-1}[s^{-\alpha_2}L\{\beta_1\sum_{n=0}^{\infty}M_n-(\phi_1+\sigma_1)E_{1n}(t)\}],$$
$$\sum_{n=0}^{\infty}E_{2(n+1)}(t)=p_3+L^{-1}[s^{-\alpha_3}L\{\beta_2\sum_{n=0}^{\infty}N_n-(\phi_2+\sigma_2)E_{2n}(t)\}], \tag{3.7}$$
$$\sum_{n=0}^{\infty}I_{1(n+1)}(t)=p_4+L^{-1}[s^{-\alpha_4}L\{\sigma_1E_{1n}(t)-(\delta+\tau_1+\gamma_1)I_{1n}(t)\}],$$
$$\sum_{n=0}^{\infty}I_{2(n+1)}(t)=p_5+L^{-1}[s^{-\alpha_5}L\{\sigma_2E_{2n}(t)-(\delta+\tau_2+\gamma_2)I_{2n}(t)\}],$$
$$\sum_{n=0}^{\infty}Q_{n+1}(t)=p_6+L^{-1}s^{-\alpha_6}L\{\tau_1I_{1n}(t)+\phi_1E_{1n}(t)+\tau_2I_{2n}(t)+\phi_2E_{2n}(t)-\theta Q_n(t)\},$$
$$\sum_{n=0}^{\infty}R_{n+1}(t)=p_7+L^{-1}[s^{-\alpha_7}L\{\theta Q_n(t)+\gamma_1I_{1n}(t)+\gamma_2I_{2n}(t)-\nu R_n(t)\}].$$

From Eq. (3.7), the initial approximations are:

$$s_0=p_1,\qquad e_{20}=p_3,\qquad i_{20}=p_5,\qquad r_0=p_7. \tag{3.8}$$
$$e_{10}=p_2,\qquad i_{10}=p_4,\qquad q_0=p_6,$$

For n = 0, the solution (3.7) reduces to

$$
\begin{aligned}
s_1 &= \{-\beta_1 p_1 p_4 - \beta_2 p_1 p_5 + \nu p_7\}\frac{t^{\alpha_1}}{\Gamma(\alpha_1+1)},\\
e_{11} &= \{\beta_1 p_1 p_4 - (\phi_1+\sigma_1)p_2\}\frac{t^{\alpha_2}}{\Gamma(\alpha_2+1)},\\
e_{21} &= \{\beta_2 p_1 p_5 - (\phi_2+\sigma_2)p_3\}\frac{t^{\alpha_3}}{\Gamma(\alpha_3+1)},\\
i_{11} &= \{\sigma_1 p_2 - (\delta+\tau_1+\gamma_1)p_4\}\frac{t^{\alpha_4}}{\Gamma(\alpha_4+1)},\\
i_{21} &= \{\sigma_2 p_3 - (\delta+\tau_2+\gamma_2)p_5\}\frac{t^{\alpha_5}}{\Gamma(\alpha_5+1)},\\
q_1 &= \{\tau_1 p_4 + \phi_1 p_2 + \tau_2 p_5 + \phi_2 p_3 - \theta p_6\}\frac{t^{\alpha_6}}{\Gamma(\alpha_6+1)},\\
r_1 &= \{\gamma_1 p_4 + \gamma_2 p_5 + \theta p_6 - \nu p_7\}\frac{t^{\alpha_7}}{\Gamma(\alpha_7+1)}.
\end{aligned}
\tag{3.9}
$$

Now, for n = 1, the solution (3.7) is reduced to

$$
\begin{aligned}
s_2 &= \{-\beta_1 p_1\{\{\sigma_1 p_2 - (\delta+\tau_1+\gamma_1)p_4\}\frac{t^{\alpha_4+\alpha_1}}{\Gamma(\alpha_4+\alpha_1+1)}\} + \{\beta_1 p_4\\
&+\beta_2 p_5\}\{\{-\beta_1 p_1 p_4 - \beta_2 p_1 p_5 + \nu p_7\}\frac{t^{2\alpha_1}}{\Gamma(2\alpha_1+1)}\} - \beta_2 p_1\{\{\sigma_2 p_3 - (\delta+\tau_2+\\
&\gamma_2)p_5\}\frac{t^{\alpha_5+\alpha_1}}{\Gamma(\alpha_5+\alpha_1+1)}\} + \nu\{\{\gamma_1 p_4 + \gamma_2 p_5 + \theta p_6 - \nu p_7\}\frac{t^{\alpha_7+\alpha_1}}{\Gamma(\alpha_7+\alpha_1+1)}\},\\
e_{12} &= \beta_1 p_1\{\sigma_1 p_2 - (\delta+\tau_1+\gamma_1)p_4\}\frac{t^{\alpha_2+\alpha_4}}{\Gamma(\alpha_2+\alpha_4+1)} + \beta_1 p_4\{-\beta_1 p_1 p_4 -\\
&\beta_2 p_1 p_5 + \nu p_7\}\frac{t^{\alpha_1+\alpha_2}}{\Gamma(\alpha_1+\alpha_2+1)} - (\phi_1+\sigma_1)\{\beta_1 p_1 p_4 - (\phi_1+\sigma_1)p_2\}\frac{t^{2\alpha_2}}{\Gamma(2\alpha_2+1)},\\
e_{22} &= \beta_2 p_1\{\sigma_2 p_3 - (\delta+\tau_2+\gamma_2)p_5\}\frac{t^{\alpha_5+\alpha_3}}{\Gamma(\alpha_5+\alpha_3+1)} + \beta_2 p_5\{-\beta_1 p_1 p_4 -\\
&\beta_2 p_1 p_5 + \nu p_7\}\frac{t^{\alpha_1+\alpha_3}}{\Gamma(\alpha_1+\alpha_3+1)} - (\phi_2+\sigma_2)\{\beta_2 p_1 p_3 - (\phi_2+\sigma_2)p_5\}\frac{t^{2\alpha_3}}{\Gamma(2\alpha_3+1)},\\
i_{21} &= \sigma_1\{\beta_1 p_1 p_4 - (\phi_1+\sigma_1)p_2\}\frac{t^{\alpha_4+\alpha_2}}{\Gamma(\alpha_4+\alpha_2+1)} - (\delta+\tau_1+\gamma_1)\{\sigma_1 p_2 -\\
&(\delta+\tau_1+\gamma_1)p_4\}\frac{t^{2\alpha_4}}{\Gamma(2\alpha_4+1)},\\
i_{22} &= \sigma_2\{\beta_2 p_1 p_3 - \sigma_2 p_5\}\frac{t^{\alpha_5+\alpha_3}}{\Gamma(\alpha_5+\alpha_3+1)} - (\delta+\tau_2+\gamma_2)\{\sigma_2 p_3 - (\delta+\tau_2+\\
&\gamma_2)p_5\}\frac{t^{2\alpha_5}}{\Gamma(2\alpha_5+1)},\\
q_2 &= \tau_1\{\sigma_1 p_2 - (\delta+\tau_1+\gamma_1)p_4\}\frac{t^{\alpha_6+\alpha_4}}{\Gamma(\alpha_6+\alpha_4+1)} + \phi_1\{\beta_1 p_1 p_4 - (\phi_1+\\
&\sigma_1)p_2\}\frac{t^{\alpha_6+t^{\alpha_2}}}{\Gamma(\alpha_6+\alpha_2+1)} + \tau_2\{\sigma_2 p_3 - (\delta+\tau_2+\gamma_2)p_5\}\frac{t^{\alpha_6+\alpha_5}}{\Gamma(\alpha_6+\alpha_5+1)} + \phi_2\{\beta_2 p_1 p_5 -\\
&(\phi_2+\sigma_2)p_3\}\frac{t^{\alpha_6+t^{\alpha_3}}}{\Gamma(\alpha_6+\alpha_3+1)} - \theta\{\tau_1 p_4 + \tau_2 p_5 - \theta p_6\}\frac{t^{2\alpha_6}}{\Gamma(2\alpha_6+1)},\\
r_2 &= \gamma_1\{\sigma_1 p_2 - (\delta+\tau_1+\gamma_1)p_4\}\frac{t^{\alpha_7+\alpha_4}}{\Gamma(\alpha_7+\alpha_4+1)} + \gamma_2\{\sigma_2 p_3 - (\delta+\tau_2+\\
&\gamma_2)p_5\}\frac{t^{\alpha_7+\alpha_5}}{\Gamma(\alpha_7+\alpha_5+1)} + \theta\{\tau_1 p_4 + \phi_1 p_2 + \tau_2 p_5 + \phi_2 p_3 - \theta p_6\}\frac{t^{\alpha_7+\alpha_6}}{\Gamma(\alpha_7+\alpha_6+1)} -\\
&\nu\{\gamma_1 p_4 + \gamma_2 p_5 + \theta p_6 - \nu p_7\}\frac{t^{2\alpha_7}}{\Gamma(2\alpha_7+1)}.
\end{aligned}
\tag{3.10}
$$

Now, considering, $\alpha_1 = \alpha_2 = \alpha_3 = \alpha_4 = \alpha_5 = \alpha_6 = \alpha_7 = \alpha$ and substituting the eq.(3.8), eq.(3.9) and eq.(3.10) in eq.(3.3). We get the series solutions:

$$S(t) = \sum_{n=0}^{2} S_n(t), \quad E_1(t) = \sum_{n=0}^{2} E_{1n}(t), \quad E_2(t) = \sum_{n=0}^{2} E_{2n}(t),$$
$$I_1(t) = \sum_{n=0}^{2} I_{1n}(t), \quad I_2(t) = \sum_{n=0}^{2} I_{2n}(t), \quad Q(t) = \sum_{n=0}^{2} Q_n(t), \quad (3.11)$$
$$R(t) = \sum_{n=0}^{2} R_n(t).$$

4 Results and Discussion

We have considered the $SE_1E_2I_1I_2QR$ model (2.3) using both the fractional Runge-Kutta fourth-ordered (FRK4) method which is indicated as blue line and the series of this model solved semi-analytically by fractional Laplace Adomian Decomposition Method (FLADM) which is mentioned by orange line. We have chosen some values based on Bangladesh's demographic and epidemiological data. To generate the graphical representation of the model, we have set values as $\delta = 0.000042$, $\beta_1 = 2.7 \times 10^{-8}$, $\beta_2 = 9.99 \times 10^{-7}$, $\sigma_1 = 0.0039$, $\sigma_2 = 0.00026$, $\phi_1 = 7 \times 10^{-6}$, $\phi_2 = 9 \times 10^{-6}$, $\tau_1 = 4.12 \times 10^{-10}$, $\tau_2 = 9.99 \times 10^{-5}$, $\nu = 1.11 \times 10^{-6}$, $\theta = 1.42 \times 10^{-5}$,and $\gamma_1 = \frac{1}{14}$, $\gamma_2 = \frac{1}{20}$ (Kim et al., 2024) with initial conditions $S(t) = 1.6 \times 10^8$ (Worldometer), $E_1(t) = 5000$, $E_2(t) = 1000$, $I_1(t) = 100$, $I_2(t) = 1$, $Q(t) = 50$, $R(t) = 5$. The approximate solution of the series (3.11) after substituting the values we get as follows:

$$S(t) = 1.6 \times 10^8 - \frac{591.84t^{\alpha}}{\Gamma(\alpha+1)} - \frac{86.9062t^{2\alpha}}{\Gamma(2\alpha+1)} + \cdots,$$
$$E_1(t) = 5000 + \frac{412.465t^{\alpha}}{\Gamma(\alpha+1)} + \frac{51.7516t^{2\alpha}}{\Gamma(2\alpha+1)} + \cdots,$$
$$E_2(t) = 1000 + \frac{159.571t^{\alpha}}{\Gamma(\alpha+1)} + \frac{33.5002t^{2\alpha}}{\Gamma(2\alpha+1)} + \cdots,$$
$$I_1(t) = 100 + \frac{12.3529t^{\alpha}}{\Gamma(\alpha+1)} + \frac{0.725742t^{2\alpha}}{\Gamma(2\alpha+1)} + \cdots,$$
$$I_2(t) = 1 + \frac{0.209858t^{\alpha}}{\Gamma(\alpha+1)} + \frac{0.0309658t^{2\alpha}}{\Gamma(2\alpha+1)} + \cdots,$$
$$Q(t) = 50 - \frac{0.0369571t^{\alpha}}{\Gamma(\alpha+1)} + \frac{0.00433908t^{2\alpha}}{\Gamma(2\alpha+1)} + \cdots,$$
$$R(t) = 5 + \frac{7.19999t^{\alpha}}{\Gamma(\alpha+1)} + \frac{0.892843t^{2\alpha}}{\Gamma(2\alpha+1)} + \cdots.$$

To analyze the population dynamics under the influence of different fractional orders, we have used Mathematica 11.3 Version and taken the values of α, which are 0.5, 0.7, 0.9, and 1 over 0 to 60 days. In fig. (1), we have shown the visual representation of the susceptible population without symptoms. fig.(1a) explains that for $\alpha = 0.5$, slight derivations between FLADM and FRK4 were observed on the other hand for $\alpha = 0.7$ they are converged. For $\alpha = 0.9$, FLADM and FRK4 initially show some convergence but eventually diverge in fig.(1c). Same outcomes present for $\alpha = 1$ in fig.(1d).

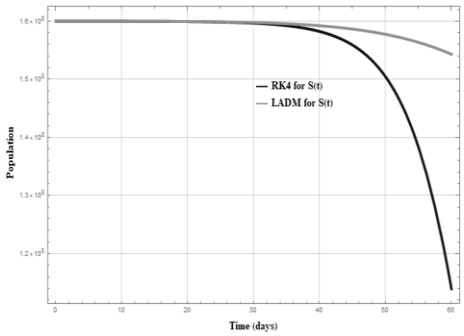

(a) Comparative visualization of analytical and numerical solutions, 0-60 days at $\alpha = 0.5$.

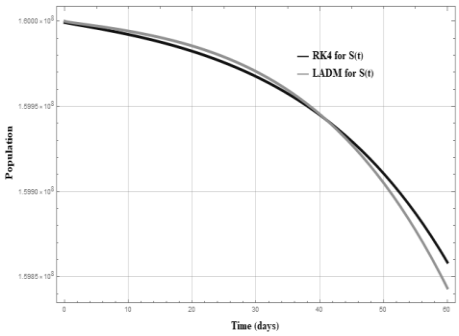

b) Comparative visualization of analytical and numerical solutions, 0-60 days at $\alpha = 0.7$.

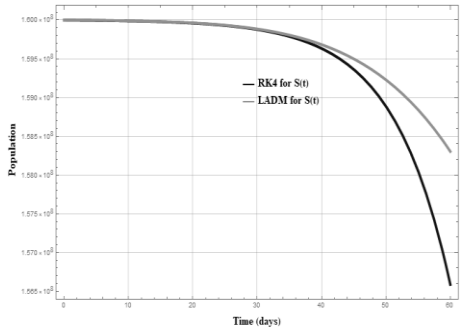

(c) Comparative visualization of analytical and numerical solutions, 0-60 days at $\alpha = 0.9$.

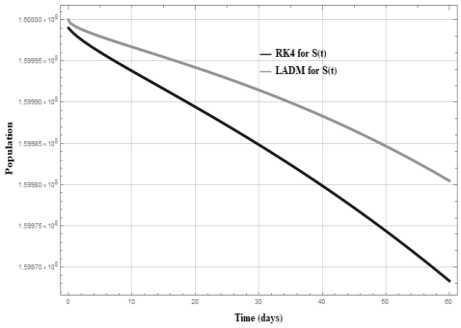

(d) Comparative visualization of analytical and numerical solutions, 0-60 days at $\alpha = 1$.

Fig. 1: Susceptible Population $S(t)$

Fig. (2) represents the exposed population who are not showing symptoms but may be infected for strain 1. As in fig.(2a) displaying variations between FLADM and FRK4 method conversely for $\alpha = 0.7$ two lines are conjunct with each other in fig.(2b). The illustration of fig.(2c) reveals the slight gap between FLADM and FRK4 technique at $\alpha = 0.9$. According to fig.(2d), the difference between the simulations increases by 3% from the previous figure.

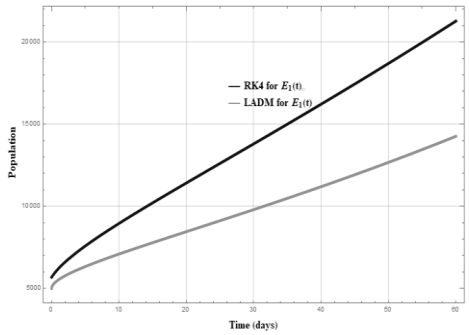

(a) Comparative visualization of analytical and numerical solutions, 0-60 days at $\alpha = 0.5$.

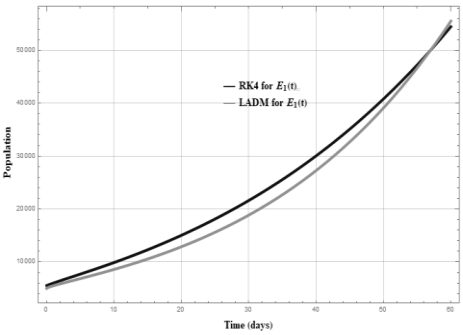

b) Comparative visualization of analytical and numerical solutions, 0-60 days at $\alpha = 0.7$.

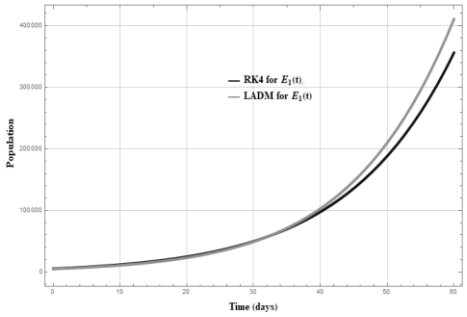

(c) Comparative visualization of analytical and numerical solutions, 0-60 days at $\alpha = 0.9$.

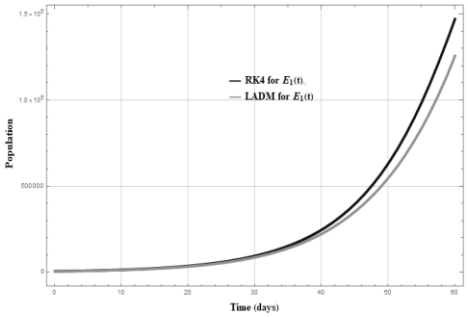

(d) Comparative visualization of analytical and numerical solutions, 0-60 days at $\alpha = 1$.

Fig. 2: Exposed Population $E_1(t)$

Fig. (3) highlights the exposed population carrying viruses but rarely exposing symptoms for strain 2. The behavior of the solution of FLADM and FRK4 technique at $\alpha = 0.5$ reflects differing trends. The graph in fig.(3b) indicates the concise view of the methods. From the fig.(3c), it can be observed that the solution fluctuates after a specific period for $\alpha = 0.9$, and the fluctuation increases when $\alpha = 1$ in fig.(3d).

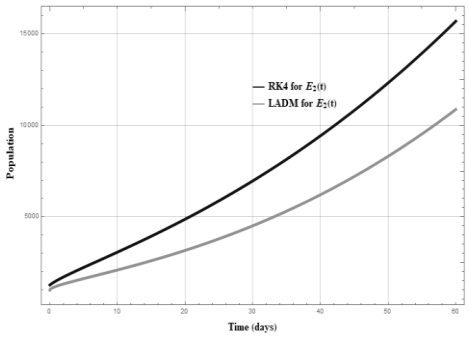

(a) Comparative visualization of analytical and numerical solutions, 0-60 days at $\alpha = 0.5$.

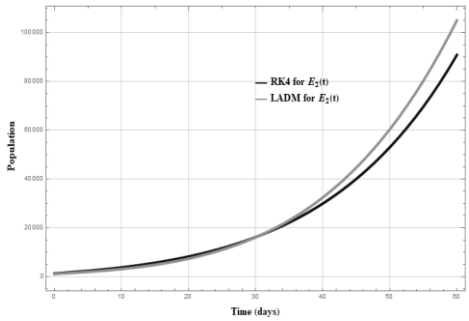

b) Comparative visualization of analytical and numerical solutions, 0-60 days at $\alpha = 0.7$.

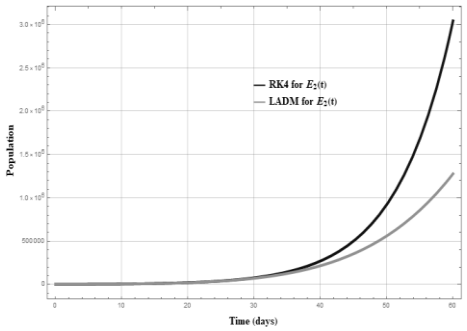

(c) Comparative visualization of analytical and numerical solutions, 0-60 days at $\alpha = 0.9$.

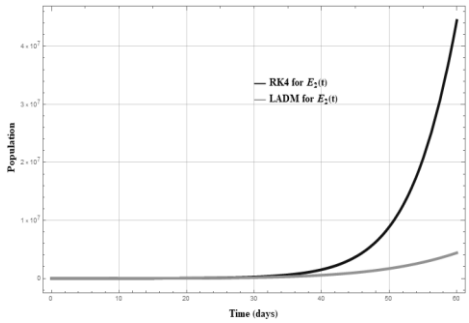

(d) Comparative visualization of analytical and numerical solutions, 0-60 days at $\alpha = 1$.

Fig. 3: Exposed Population $E_2(t)$

The visual representation of fig. (4) reveals the behavior of an infected population already symptomatic for strain 1. As depicted in the fig.(4a), the methods deviate significantly from each other at $\alpha = 0.5$. Oppositely, the fig.(4b) displays almost identical behavior for $\alpha = 0.7$ as they progress over time. Fig.(4c) portraying that the two methods initially approached each other at $\alpha = 0.9$ but then moved apart, and in fig.(4d), divergency has increased at $\alpha = 1$.

The presented fig. (5) demonstrates the infected population exhibiting virus symptoms for strain 2. The diagram of fig.(5a) reflects that the two approaches deviate significantly from each other for $\alpha = 0.5$ alternatively at $\alpha = 0.7$ the unification of the two methods occurs as time progresses which is visible in fig.(5b). The visual manifest of fig.(5c) declares that at $\alpha = 0.9$ an initial convergence transitioned into divergence, and the distance has grown as the value of α increased to 1 that explained in fig.(5d).

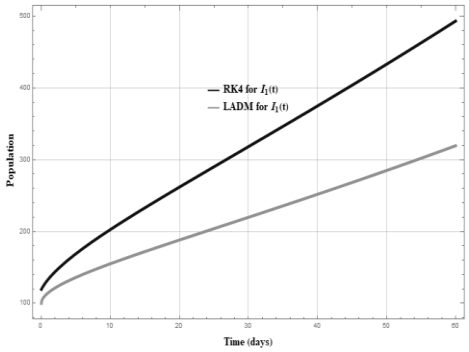

(a) Comparative visualization of analytical and numerical solutions, 0-60 days at $\alpha = 0.5$.

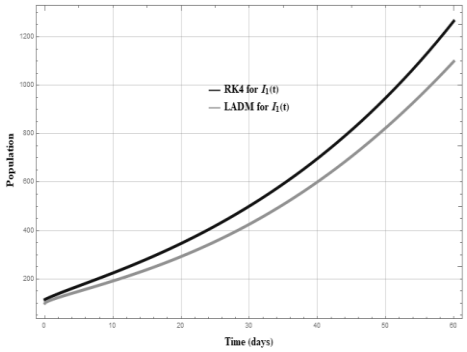

b) Comparative visualization of analytical and numerical solutions, 0-60 days at $\alpha = 0.7$.

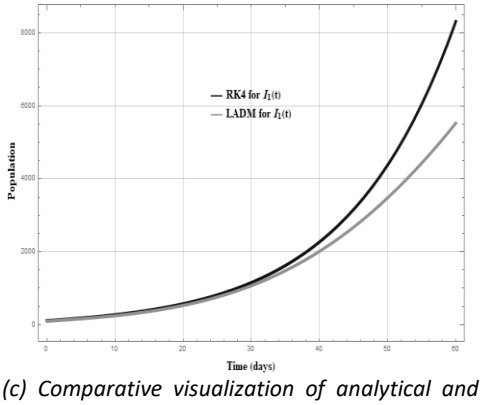

(c) Comparative visualization of analytical and numerical solutions, 0-60 days at $\alpha = 0.9$.

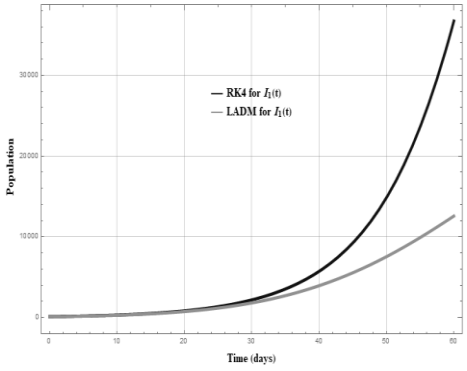

(d) Comparative visualization of analytical and numerical solutions, 0-60 days at $\alpha = 1$.

Fig. 4: Infected Population $I_1(t)$

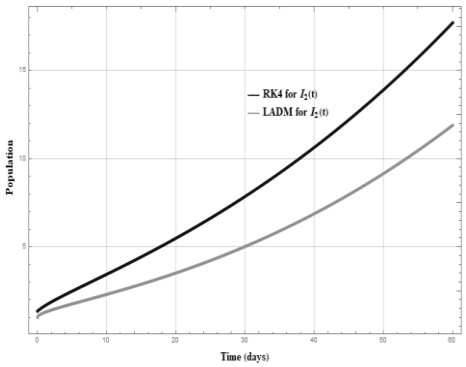

(a) Comparative visualization of analytical and numerical solutions, 0-60 days at $\alpha = 0.5$.

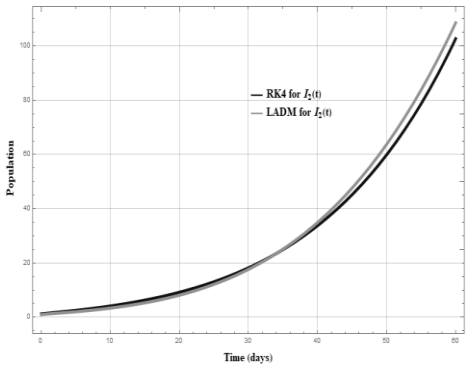

b) Comparative visualization of analytical and numerical solutions, 0-60 days at $\alpha = 0.7$.

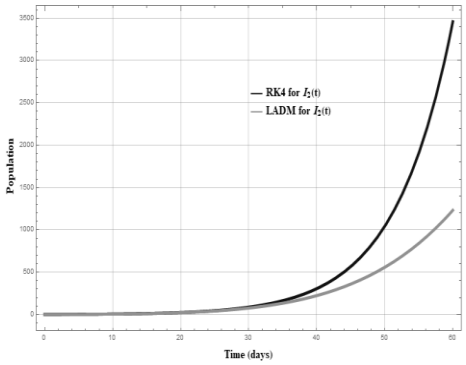

(c) Comparative visualization of analytical and numerical solutions, 0-60 days at $\alpha = 0.9$.

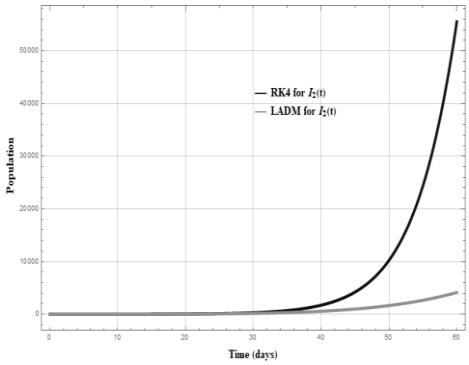

(d) Comparative visualization of analytical and numerical solutions, 0-60 days at $\alpha = 1$.

Fig. 5: Infected Population $I_2(t)$

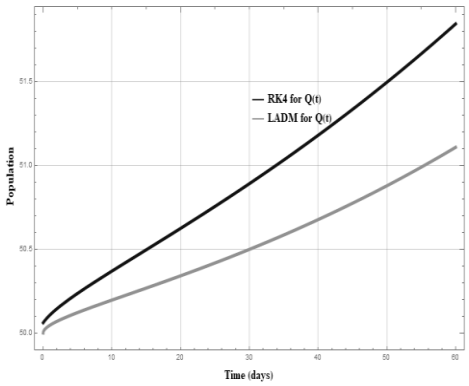

(a) Comparative visualization of analytical and numerical solutions, 0-60 days at $\alpha = 0.5$.

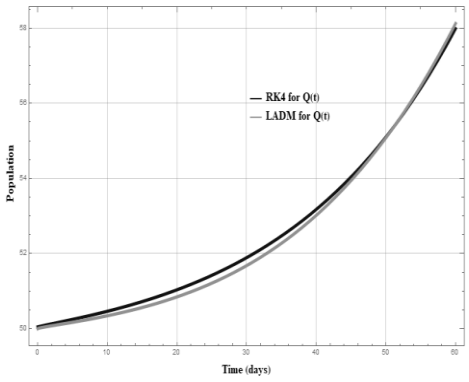

b) Comparative visualization of analytical and numerical solutions, 0-60 days at $\alpha = 0.7$.

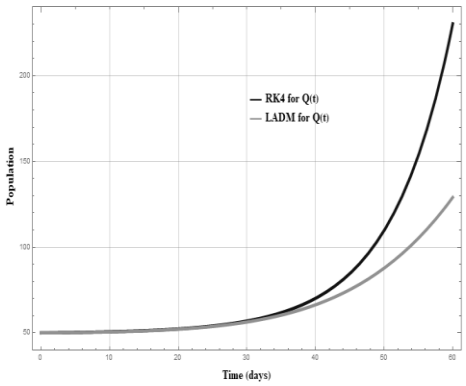

(c) Comparative visualization of analytical and numerical solutions, 0-60 days at $\alpha = 0.9$.

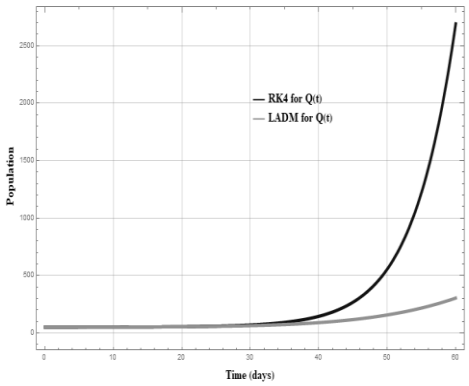

(d) Comparative visualization of analytical and numerical solutions, 0-60 days at $\alpha = 1$.

Fig. 6: Quarantine Population $Q(t)$

The plot explains the quarantine population considered hospitalized or home isolation for identifying the diseases in fig. (6). According to fig.(6a), the FRK4 method and FLADM no longer align with each other and move apart from the initial point at $\alpha = 0.5$. Inversely, for $\alpha = 0.7$ primarily, the two methods exhibit close agreement. Noticeable deviation occurs as the computation progresses for $\alpha = 0.9$ for fig.(6c) in a similar fashion for fig.(6d), the methods are convergence for a brief period then divergence occurred at $\alpha = 1$. From fig. (7), it can be observed that the approach of two methods for the population who have recovered from the diseases. The results of the two methods start to differ noticeably in the fig.(7a) at $\alpha = 0.5$. Reciprocally, for $\alpha = 0.7$, a minimal discrepancy is observed in fig.(7b) between the results of FLADM and FRK4. From the fig.(7c) at $\alpha = 0.9$ convergence, the methods stay side by side, and for $\alpha = 1$ there has early convergence, but divergence reappeared afterward that, visible in fig.(7d).

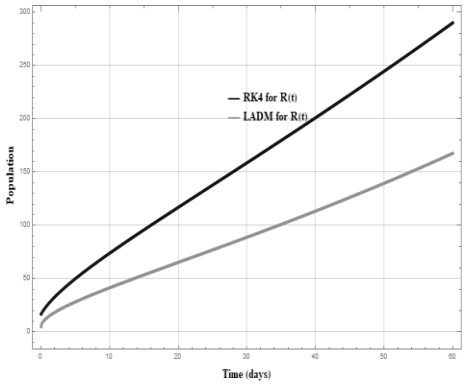

(a) Comparative visualization of analytical and numerical solutions, 0-60 days at $\alpha = 0.50$.

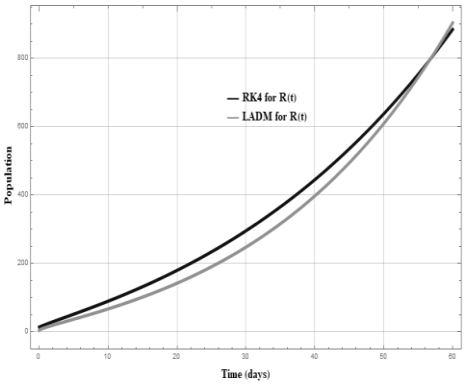

b) Comparative visualization of analytical and numerical solutions, 0-60 days at $\alpha = 0.70$.

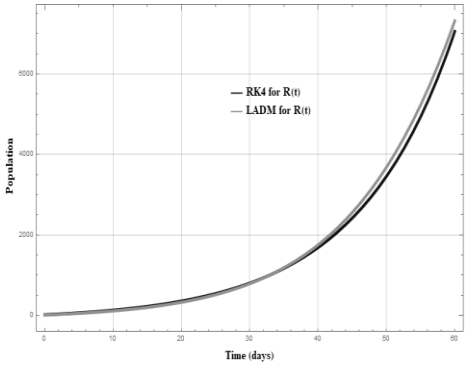

(c) Comparative visualization of analytical and numerical solutions, 0-60 days at $\alpha = 0.90$.

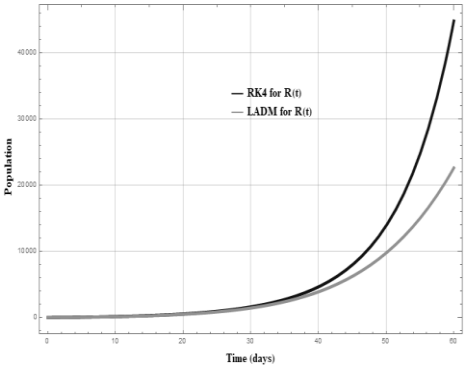

(d) Comparative visualization of analytical and numerical solutions, 0-60 days at $\alpha = 1$.

Fig. 7: Recovered Population $R(t)$

5 Conclusion

In this present study, we deployed a fractional-order mathematical model to examine the co-dynamics of COVID-19 strains. Approximate analytical solutions were obtained via the FLADM, and the FRK4 technique was used to compare the results. The impact of memory on population dynamics can be evaluated after varying the fractional order of α between 0.5, 0.7, 0.9, and 1. Particularly at α = 0.7, the solutions obtained by FLADM and FRK4 show a strong agreement with negligible differences between the two methods, which can explain the precision as well as resilience of LADM in capturing the fractional dynamics of disease spread. Our findings demonstrate that the fractional order has a significant impact on the behavior of the system. So, we can say that the LADM is proved to be an efficient and reliable method for solving FDEs, particularly for epidemiological applications. Future work could explore the application of LADM to more complex models, including those with multiple strains, vaccination strategies, and varying transmission rates under fractional dynamics.

Acknowledgment

The first author gratefully acknowledges financial support from the Ministry of Science and Technology, Government of the People's Republic of Bangladesh, through the NST Fellowship (2024–2025) for her PhD studies (Grant No. 39.00.0000.012.02.009.24.30; Merit No. 06; Serial No. 03; dated 30 January 2025).

References

Abdulrhman, T. (2025). Stability analysis of fractional chaotic and fractional-order hyperchain systems using Lyapunov functions. European Journal of Pure and Applied Mathematics, 18(1), 5576.

Abraham, S., Dangbé, E., Irépran, D., & Perasso, A. (2025). Mathematical modeling and analysis of the effect of vaccination and temperature on the dynamic transmission of coronavirus disease 2019 (COVID-19). International Journal of Dynamics and Control, 13(5), 186.

Agarwal, R., Airan, P., & Agarwal, R. P. (2024). Exploring the landscape of fractional-order models in epidemiology: A comparative simulation study. Axioms, 13(8).

Ali, M., Guma, F. E., Qazza, A., Saadeh, R., Alsubaie, N. E., Althubyani, M., & Abdoon, M. A. (2024). Stochastic modeling of influenza transmission: Insights into disease dynamics and epidemic management. Partial Differential Equations in Applied Mathematics, 11, 100886.

Ambalarajan, V., Mallela, A. R., Dhandapani, P. B., Sivakumar, V., Leiva, V., & Castro, C. (2025). Multi-strain COVID-19 dynamics with vaccination strategies: Mathematical modeling and case study. Alexandria Engineering Journal, 119, 665–684.

Aron, J. L., & Schwartz, I. B. (1984). Seasonality and period-doubling bifurcations in an epidemic model. *Journal of Theoretical Biology, 110*(4), 665–679.

Baba, I. A., Rihan, F. A., & Hincal, E. (2024). Analyzing co-infection dynamics: A mathematical approach using fractional-order modeling and Laplace–Adomian decomposition. *Journal of Biosafety and Biosecurity, 6*(2), 113–124.

Barros, L. C. D., Lopes, M. M., Pedro, F. S., Esmi, E., Santos, J. P. C. D., & Sánchez, D. E. (2021). The memory effect on fractional calculus: An application in the spread of COVID-19. *Computational and Applied Mathematics, 40*, 1–21.

Bentaleb, D., Khatar, Z., & Amine, S. (2024). Epidemiological modeling of monkeypox clades: A dual-strain SEIR approach with stability, bifurcation, and sensitivity analysis. *Modeling Earth Systems and Environment*, 1–15.

Betti, M., Bragazzi, N., Heffernan, J., Kong, J., & Raad, A. (2021). Could a new COVID-19 mutant strain undermine vaccination efforts? A mathematical modelling approach. *Vaccines, 9*(6), 592.

Bhuju, G., Phaijoo, G. R., & Gurung, D. B. (2022). Sensitivity and bifurcation analysis of fuzzy SEIR–SEI dengue disease model. *Journal of Mathematics, 2022*, 1927434.

Bouissa, A., Azouagh, N., & Tsouli, N. (2025). Mathematical analysis of an SIRS fractional-order model with competition involving two pathogen strains: An application to COVID-19. *Japan Journal of Industrial and Applied Mathematics*, 1–26.

Centers for Disease Control and Prevention. (2023, January 10). *How to protect yourself & others*. https://www.cdc.gov/covid/prevention/

Chang, A. Y., Cullen, M. R., Harrington, R. A., & Barry, M. (2021). The impact of COVID-19 on noncommunicable disease patients and health systems. *Journal of Internal Medicine, 289*(4), 450–462.

Chowdhury, M. A., Hossain, N., Kashem, M. A., Shahid, M. A., & Alam, A. (2020). Immune response in COVID-19: A review. *Journal of Infection and Public Health, 13*(11), 1619–1629.

Chu, Y. M., Jneid, M., Chaouk, A., Inc, M., Rezazadeh, H., & Houwe, A. (2024). Local time fractional reduced differential transform method for solving local time fractional telegraph equations. *Fractals, 32*(4), 2340128.

Farman, M., Saleem, M. U., Ahmad, A., & Ahmad, M. O. (2018). Analysis and numerical solution of SEIR epidemic model of measles with non-integer time fractional derivatives using Laplace–Adomian decomposition method. *Ain Shams Engineering Journal, 9*(4), 3391–3397.

Ghosh, A., Roy, S., Mondal, H., Biswas, S., & Bose, R. (2022). Mathematical modelling for decision making of lockdown during COVID-19. *Applied Intelligence, 52*(1), 699–715.

Haq, F., Shah, K., ur Rahman, G., & Shahzad, M. (2018). Numerical solution of fractional-order smoking model via Laplace–Adomian decomposition method. *Alexandria Engineering Journal, 57*(2), 1061–1069.

Heim, N., Berger, M., Wiedemeyer, V., Reich, R., & Martini, M. (2019). A mathematical approach improves the predictability of length of hospitalization due to acute odontogenic infection: A retrospective investigation of 303 patients. *Journal of Cranio-Maxillofacial Surgery, 47*(2), 334–340.

Huo, X., Chen, J., & Ruan, S. (2021). Estimating asymptomatic, undetected and total cases for the COVID-19 outbreak in Wuhan: A mathematical modeling study. *BMC Infectious Diseases, 21*(1), 476.

Islam, M. R., Mahmud, F., & Akbar, M. A. (2024). Insights into the Ebola epidemic model and vaccination strategies: An analytical approximate approach. *Partial Differential Equations in Applied Mathematics, 11*, 100799.

Islam, M., & Akbar, M. A. (2024). A study on the fractional-order COVID-19 SEIQR model and parameter analysis using homotopy perturbation method. *Partial Differential Equations in Applied Mathematics, 12*, 100960.

Ivorra, B., Ferrández, M. R., Vela-Pérez, M., & Ramos, A. M. (2020). Mathematical modeling of the spread of coronavirus disease 2019 (COVID-19) taking into account undetected infections: The case of China. *Communications in Nonlinear Science and Numerical Simulation, 88*, 105303.

Jacobs, J. L., Haidar, G., & Mellors, J. W. (2023). COVID-19: Challenges of viral variants. *Annual Review of Medicine, 74*(1), 31–53.

Kermack, W. O., & McKendrick, A. G. (1927). A contribution to the mathematical theory of epidemics. *Proceedings of the Royal Society of London. Series A, 115*(772), 700–721.

Kim, Y. R., Min, Y., & Okogun-Odompley, J. N. (2024). A mathematical model of COVID-19 with multiple variants of the virus under optimal control in Ghana. *PLOS ONE, 19*(7), e0303791.

Minhós, F., Raza, A., & Shafique, U. (2025). Mathematical modeling and dynamics of gonorrhoea epidemic within stochastic fractional delay differential equations. *Modeling Earth Systems and Environment, 11*(2), 1–16.

Mondal, J., & Khajanchi, S. (2022). Mathematical modeling and optimal intervention strategies of the COVID-19 outbreak. *Nonlinear Dynamics, 109*(1), 177–202.

Negi, S. S., Sharma, N., & Baskonus, H. M. (2024). Dual-strain dynamics of COVID-19 variants in India: Modeling, analysis, and implications for pandemic control. *Gene, 926*, 148586.

Panovska-Griffiths, J., Swallow, B., Hinch, R., Cohen, J., Rosenfeld, K., Stuart, R. M., … COVID-19 Genomics UK (COG-UK) Consortium. (2022). Statistical and agent-based modelling of the transmissibility of SARS-CoV-2 variants in England. *Philosophical Transactions of the Royal Society A, 380*(2233), 20210315.

Prakash Raj, M., Venkatesh, A., Arun Kumar, K., & Manivel, M. (2025). Mathematical modeling of the co-infection dynamics of dengue and malaria using delay differential equations. *Advanced Theory and Simulations, 8*(2), 2400609.

Redondo, E., Nicoletta, V., Bélanger, V., Garcia-Sabater, J. P., Landa, P., Maheut, J., … Ruiz, A. (2023). A simulation model for predicting hospital occupancy for COVID-19 using archetype analysis. *Healthcare Analytics, 3*, 100197.

Riaz, M., Ali, Z., Din, R. U., Ahmad, S., Abodayeh, K., & Sarwar, M. (2025). Mathematical modeling with two strains to investigate evolution of COVID-19. *European Journal of Pure and Applied Mathematics, 18*(2), 6001.

Saber, S., Solouma, E., Alharb, R. A., & Alalyani, A. (2025). Chaos in fractional-order glucose–insulin models with variable derivatives. *Fractal and Fractional, 9*(3), 149.

Safi, M. A., & Gumel, A. B. (2011). Mathematical analysis of a disease transmission model with quarantine, isolation and an imperfect vaccine. *Computers & Mathematics with Applications, 61*(10), 3044–3070.

Thompson, R. N. (2020). Epidemiological models are important tools for guiding COVID-19 interventions. *BMC Medicine, 18*, 1–4.

Upadhyay, R. K., Barman, A. K., Das, P., & Panda, B. (2025). Investigation of complexity in extracellular matrix-induced cancer dynamics under deterministic and stochastic frameworks. *Nonlinear Dynamics*, 1–36.

White, M. T., Verity, R., Churcher, T. S., & Ghani, A. C. (2015). Vaccine approaches to malaria control and elimination: Insights from mathematical models. *Vaccine, 33*(52), 7544–7550.

World Health Organization. (n.d.). *Coronavirus*. Retrieved April 30, 2025, from https://www.who.int/health-topics/coronavirus

Worldometer. (n.d.). *COVID-19 coronavirus pandemic*. Retrieved January 11, 2025, from https://www.worldometers.info/coronavirus/

Wu, J. T., Leung, K., & Leung, G. M. (2020). Nowcasting and forecasting the potential domestic and international spread of the 2019-nCoV outbreak. *The Lancet, 395*(10225), 689–697.

Yaagoub, Z., Farah, E. M., & Ahmad, S. (2025). Three-strain epidemic model for influenza virus involving fractional derivative and treatment. *Journal of Applied Mathematics and Computing, 71*(1), 1247–1266

Zhang, X., An, Q., & Moussaoui, A. (2025). Effect of density-dependent diffusion on a diffusive predator–prey model in spatially heterogeneous environment. *Mathematics and Computers in Simulation, 227*, 1–18.